Solar Energy Materials and Solar Cells 186 (2018) 291–299

Contents lists available at ScienceDirect

Solar Energy Materials and Solar Cells

journal homepage: www.elsevier.com/locate/solmat

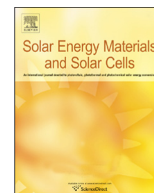

BBr_3 diffusion with second deposition for laser-doped selective emitters from borosilicate glass

Elmar Lohmüller*, Sabrina Lohmüller (née Werner), Nico Wöhrle, Udo Belledin, Andreas Wolf

Fraunhofer Institute for Solar Energy Systems (ISE), Heidenhofstraße 2, 79110 Freiburg, Germany

ARTICLE INFO

Keywords:
BBr_3 diffusion
Second deposition
Borosilicate glass (BSG)
Selective emitter
Laser doping

ABSTRACT

We study a boron tribromide (BBr_3) diffusion process with second deposition realized by active nitrogen flow through the BBr_3 bubbler at the end of the process with respect to laser doping. Compared to the reference BBr_3 diffusion without second deposition, the new BBr_3 diffusion provides a two times higher boron dose within the borosilicate glass (BSG)/silicon dioxide (SiO_2) stack layer grown on the silicon surface. The second deposition leads to both thinning of the intermediate SiO_2 layer and 11 nm-growth of the BSG layer, which results in an 8 nm thicker BSG/SiO_2 stack layer with a total thickness of 42 nm. These altered properties of the BSG/SiO_2 layer facilitate the formation of laser-doped selective boron emitters, while the second deposition hardly affects the as diffused charge carrier concentration profile. The obtained emitter properties, sheet resistance $R_{sh} \approx 100\,\Omega$/sq and emitter dark saturation current density $j_{0e} \approx 25$ fA/cm^2 (textured surface, Al_2O_3/SiN_X passivation) for the photoactive part of the emitter are not affected by the introduced second deposition step. For the laser-doped part of the emitter, the charge carrier concentration after laser doping is higher for the BBr_3 diffusion with second deposition resulting in stronger local doping with up to 10 Ω/sq lower R_{sh}. The application of an analytical model to calculate specific contact resistances ρ_C in dependence of e.g. dopant concentration of the laser-doped profiles and crystallite penetration depth d_{cryst} reveals that ρ_C is expected to benefit largely from the altered profile shapes due to laser doping for the BBr_3 diffusion with second deposition. A relative decrease in ρ_C of up to 90% and 50% is found for small d_{cryst} (depth of several tens of nm) and large d_{cryst} (depth of several hundreds of nm), respectively. Another potential advantage of the second deposition holds for emitter dark saturation current densities at the metal-silicon interface $j_{0,met}$. A 3D simulation model that is based on metal crystallites penetrating into the emitter considering the different doping profiles after laser processing yields a $j_{0,met} \approx 740$ fA/cm^2 for small d_{cryst} that is 14% relatively lower for the BBr_3 diffusion with second deposition.

1. Introduction

The emitter dark saturation current density j_{0e} for the passivated front side boron emitter in n-type silicon solar cells reduces drastically when lowering the maximum charge carrier concentration N_{max} present at or close to the silicon surface [1–7]. To form boron emitters, commonly tube furnace diffusion processes using boron tribromide (BBr_3) as liquid dopant precursor are applied. To lower N_{max} in the resulting doping profile, several adaptions within the BBr_3 diffusion process can be considered. One very promising and industrially relevant approach is the implementation of a post-oxidation step in oxygen (O_2) ambient at the end of the process sequence [4,8]. Applying post-oxidation, segregation of boron into the growing silicon dioxide (SiO_2) layer on the silicon surface and oxidation-enhanced diffusion of boron lead to a decrease in N_{max} and redistribution of boron dopants [9,10].

Despite reductions in N_{max}, low specific contact resistance ρ_C in the range of a few mΩ cm^2 is maintained for screen-printed and fired silver-aluminum (Ag-Al) contacts [3,6,11]. As example, Ref. [6] reports on $N_{max} = 1.8{\cdot}10^{19}$ cm^{-3} and $\rho_C \approx 3$ mΩ cm^2 for commercial screen-printed and fired 70 µm-wide Ag-Al contact fingers. However, such lowly-doped boron emitters result in strongly increased local charge carrier recombination activity at the Ag-Al contacts with values for the dark saturation current density below the metal contacts $j_{0,met}$ of up to several thousands of fA/cm^2 [2,12–15]. These high $j_{0,met}$ values lead to severe open-circuit voltage losses and thus, the energy conversion efficiencies of the associated devices are limited by the charge carrier recombination at the emitter-metal interface [2,13–18]. One possible explanation for the high $j_{0,met}$ observed for Ag-Al contacts – which is widespread within the photovoltaic community – is the fact that Ag-Al contacts feature large and deep metal crystallites at the interface

* Corresponding author.
E-mail addresses: elmar.lohmueller@ise.fraunhofer.de (E. Lohmüller), sabrina.lohmueller@ise.fraunhofer.de (S. Lohmüller (née Werner)), nico.woehrle@ise.fraunhofer.de (N. Wöhrle), udo.belledin@ise.fraunhofer.de (U. Belledin), andreas.wolf@ise.fraunhofer.de (A. Wolf).

https://doi.org/10.1016/j.solmat.2018.06.042
Received 12 March 2018; Received in revised form 21 June 2018; Accepted 23 June 2018
0927-0248/ © 2018 Elsevier B.V. All rights reserved.

between the Ag-Al bulk contact and the boron-doped surface [12,13,19–23]. These metal crystallites reach depths up to a few microns. To significantly decrease charge carrier recombination at the interface of emitter and Ag-Al contacts, e.g., deep doping profiles and/or high N_{max} values are necessary [15,16].

On the other hand, low N_{max} and rather shallow profiles are favorable for the photoactive passivated boron emitter to ensure low j_{0e} and a high blue response for most of the front side. Hence, the challenge is to provide two different emitter properties on the same wafer surface. An approach that can fulfill both requirements is the application of a laser-doped selective boron emitter. Laser doping out of a doped layer present on the silicon surface is a method for realization of selective emitter structures [24–32]. Often, doped layers grown during tube furnace diffusion processes serve as dopant source for subsequent laser doping. The local laser doping from the phosphosilicate glass (PSG) and SiO_2 stack layer [26,27,30,33] that grows on the silicon surface during tube furnace diffusion using phosphorus oxychloride ($POCl_3$) is meanwhile state-of-the-art for forming selective phosphorus-doped emitters for p-type silicon solar cells [26,28,31,34]. Similarly, in case of n-type silicon solar cells, local laser doping from the borosilicate glass (BSG) and SiO_2 stack layer grown on the silicon surface during BBr_3 diffusion has already been applied for forming selective boron emitters [29,32,35].

We recently demonstrated the incorporation of a second deposition step with active nitrogen (N_2) flow through the BBr_3 bubbler at the end of an advanced BBr_3 diffusion process providing additional boron in the BSG/SiO_2 stack layer that positively affects the laser doping [32]. The results published in Ref. [32] form the basis for further investigations that are carried out in the present paper. Hence, in the present paper, we review some of the results from Ref. [32] and we show further details concerning the studies of the BSG/SiO_2 stack layer. As continuation of the previous investigations, we examine the resulting doping profiles within the silicon in terms of specific contact resistance ρ_C and charge carrier recombination $j_{0,met}$ at the emitter-metal interface. These examinations are based on an analytical model for calculation of ρ_C [19] and a 3D simulation model for calculation of $j_{0,met}$ [15].

2. Experimental

2.1. BBr_3 diffusion processes

The BBr_3 diffusion processes are performed under atmospheric pressure in an industrial tube furnace. We study two BBr_3 diffusion processes, both of which feature a short post-oxidation [6]. The selected reference process “Ref” yields very low emitter dark saturation current density $j_{0e} \approx 25\,fA/cm^2$ at a sheet resistance $R_{sh} \approx 110\,\Omega/sq$ for alkaline textured and aluminum oxide (Al_2O_3)/silicon nitride (SiN_X) passivated surface after activation in a contact firing process [32]. The second BBr_3 diffusion process, referred to as “2nd dep” in the following, is identical to the “Ref”-process except of a second deposition step. This second deposition step is identical to the initial deposition step performed before drive-in and is realized by active N_2 gas flow through the BBr_3 bubbler directly after the post-oxidation temperature plateau at the end of reference process “Ref”.

2.2. Sample fabrication

Conventional n-type Czochralski-grown silicon (Cz-Si) wafers with edge length $L_{edge} = 156\,mm$ are either wet-chemically saw damage etched or wet-chemically alkaline textured before BBr_3 diffusion.

The saw damage etched wafers serve for studying several characteristics of the BSG/SiO_2 stack layers grown during the two BBr_3 diffusion processes such as thickness, structural composition, and boron content. Ellipsometry measurements determine the total glass layer thickness. For studying the selectivity in etching rate of the BSG and SiO_2 layers, we apply the etching procedure that is described in detail in Ref. [33] using 0.1% hydrofluoric acid (HF) solution. The alkaline textured wafers serve three purposes: (i) determination of depth-dependent charge carrier concentration profiles by electrochemical capacitance voltage (ECV) measurements [36,37], (ii) determination of sheet resistances R_{sh} by four point probe (4pp) technique, and (iii) extraction of emitter dark saturation current densities j_{0e} on symmetric Al_2O_3/SiN_X passivated carrier lifetime samples after firing [38].

Table 1
Overview of the settings used for full-area laser doping from the BSG/SiO_2 stack layer system grown during BBr_3 tube furnace diffusion (d_{pulse}: pulse-to-pulse distance, d_{line}: line distance, E_p: laser pulse energy).

	d_{pulse} (µm)	d_{line} (µm)	E_p (µJ)
Setting 1	15	25	74
Setting 2	15	25	120
Setting 3	32	35	120

For laser doping from the BSG/SiO_2 stack layer after BBr_3 diffusion, we apply a pulsed ultraviolet nanosecond frequency-tripled Nd:YVO_4 solid-state laser (wavelength $\lambda_{laser} = 355\,nm$, pulse length $\tau_{laser} \approx 25\,ns$) [25,28]. For ECV as well as 4pp measurements, $2 \times 2\,cm^2$-large full-area laser-doped test fields are formed on different positions on one side of separate textured samples. We apply three different laser settings as summarized in Table 1. Non-lasered fields serve as reference. ECV measurements follow the glass layer removal in HF. For the symmetric lifetime samples, we arrange $4 \times 4\,cm^2$-large full-area laser-doped test fields symmetrically on both sides of textured samples.

2.3. Analysis of the BSG/SiO_2 stack layer after BBr_3 diffusion

The investigations of the BSG/SiO_2 stack layers are performed on saw damage etched surface, as ellipsometry measurements are more reliable than on texture. As the layer growth is depending among others on crystal orientation, the layer thickness on saw damage etched surface might be different to those on alkaline textured surface. However, the trend and the general findings also hold for the textured samples.

The total stack layer thickness d over the complete wafer surface is rather inhomogeneous for the studied BBr_3 diffusion processes with a standard deviation between 10% and 20%. The measured mean total stack layer thicknesses increases due to the second deposition step from $d = (34 \pm 5)\,nm$ for BBr_3 diffusion “Ref” to $d = (42 \pm 8)\,nm$ for process “2nd dep”. Due to this non-uniformity, the determined individual layer thicknesses of the BSG and SiO_2 layers might be prone to a larger error than the results from Ref. [33]. Nevertheless, we think the etching procedure is still a suitable approach for investigation of the present BSG/SiO_2 stack layers when plotting the etching removal Δd (Fig. 1) instead of the remaining total layer thickness d. By using Δd, the different initial total layer thicknesses do not dominate the resulting graph and the etching rate of the outer BSG layer can be determined more accurately; especially for short etching times t – meaning low removal Δd.

Fig. 1 shows the results of the stepwise etching procedure of the BSG/SiO_2 stack layers. The abrupt change occurring in etching rate indicates the presence of a two-layer system – namely BSG and SiO_2 – on the silicon surface, whose presence is in agreement with other publications [39–41]. The BSG etching rates are $r_{BSG} = (1.7 \pm 0.1)\,nm/min$ and $r_{BSG} = (3.1 \pm 0.2)\,nm/min$ for “Ref” and “2nd dep”, respectively. Compared to our respective findings for phosphosilicate glass (PSG)/SiO_2 stack layers present after phosphorus oxychloride ($POCl_3$) diffusion [33], the BSG etching rates are significantly lower than those observed for PSG layers from $POCl_3$ diffusion, which is consistent with literature [39,41]. The roughly twice as large BSG etching rate r_{BSG} for BBr_3 diffusion “2nd dep” compared to that of “Ref” indicates a significantly higher boron concentration within

Download English Version:

https://daneshyari.com/en/article/6533886

Download Persian Version:

https://daneshyari.com/article/6533886

Daneshyari.com